RSC Advances

ROYAL SOCIETY OF CHEMISTRY

www.rsc.org/advances

The Number Density Effect of N-Substituted Dyes on the TiO_2 Surface in Dye Sensitized Solar Cells: A Theoretical study

The bulky of the N-Substituted donor moiety reduces the number density of the adsorbed **Dye3** on the surface dramatically, corresponding to poorer energy conversion efficiency of 3.91% in **Dye3** compared to the significantly better performance of 5.45% in **Dye2**.

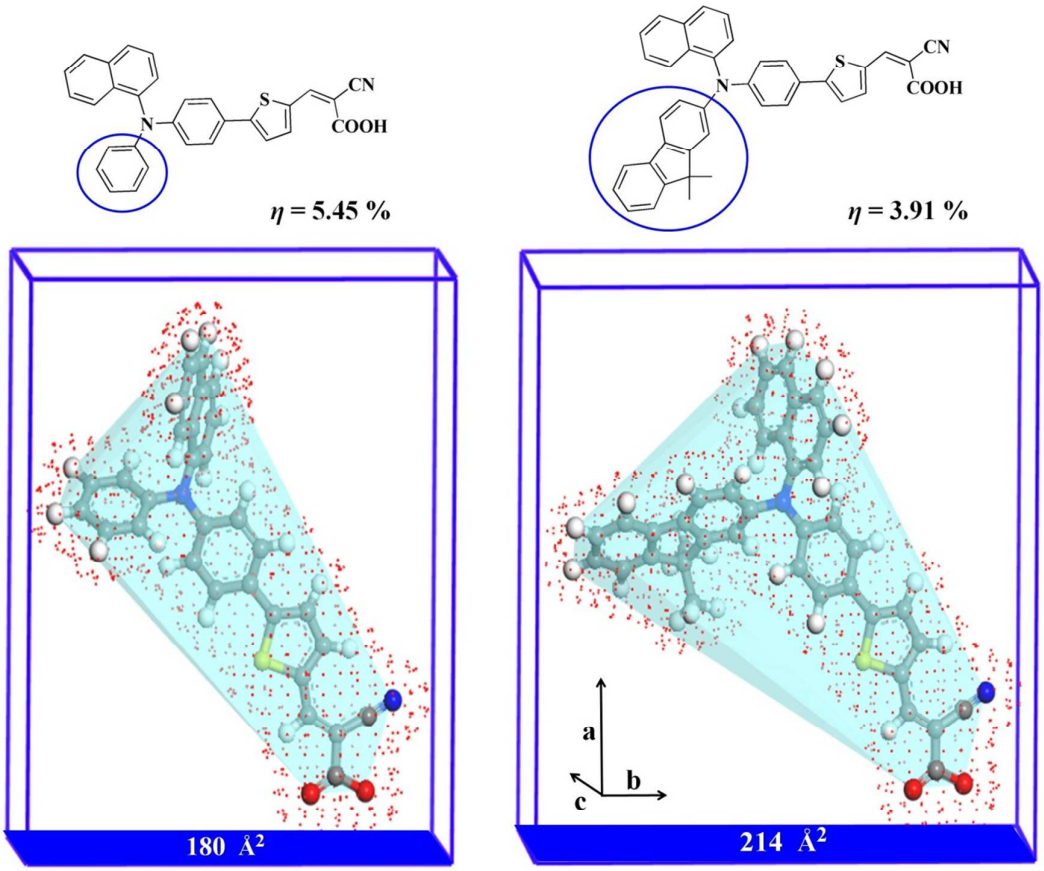

The Number Density Effect of N-Substituted Dyes on the TiO_2 Surface in Dyes Sensitized Solar Cells: A Theoretical Study

Yaowarat Surakhot[1], Rattanawalee Rattanawan[1], Kritsada Ronyhut[1], Ponlawat Mangsachart[1] Taweesak Sudyoadsuk[1], Vinich Promarak[2], Supawadee Namuangruk[3], Nawee Kungwan[4] and Siriporn Jungsuttiwong[1*]

[1]Center for Organic Electronic and Alternative Energy, Department of Chemistry and Center of Excellence for Innovation in Chemistry, Faculty of Science, Ubon Ratchathani University, Ubon Ratchathani, 34190 Thailand

[2] School of Chemistry and Center for Innovation in Chemistry, Institute of Science, Suranaree University of Technology, Muang District, Nakhon Ratchasima 30000, Thailand.

[3] National Nanotechnology Center, National Science and Technology Development Agency, 111 Paholyothin Rd., Klong Luang, Pathumthani, 12120, Thailand

[4]Department of Chemistry, Faculty of Science, Chiang Mai University, Chiang Mai 50200, Thailand

**Corresponding author: Tel.: +66816922125*

E-mail: siriporn.ubu@gmail.com

Abstract

A series of organic dyes, containing N-Substituted carbazole, diarylamine-naphthalene, and diarylamine-fluorene donor for **Dye1**, **Dye2,** and **Dye3**, respectively, and cyanoacrylic acid acceptor bridged by thiophene fragment for Dye Sensitized Solar Cells (DSCs) applications, is successfully investigated by DFT and TDDFT. Among these dyes, **Dye3,** with the strongest electron donating ability, shows the most red shift in the UV-Vis absorption spectrum. Moreover, **Dye3**@$(TiO_2)_{38}$ complex shows stronger adsorption energy of -19.54 kcal/mol. Nevertheless, **Dye2** has shown the best photovoltaic performance. We measured the molecular volume and molecular width based on the geometries from the PBE functional, together with the Double-Numerical with polarization performed in the DMol^3 program, to investigate the effect of N-substituted donors on the number density of the adsorbed dye, on the TiO_2 surface. We found that the bulkiness of the N-substituted donor in **Dye3** can dramatically reduce the number density of the adsorbed on the surface. The molecular width and projected area of **Dye3** are calculated to be 15.980 Å of 214 Å^2, respectively, indicating the more bulky-structure compared to **Dye2** (molecular width =14.505 Å and projected area = 180 Å^2) which corresponds to the dye uptake of **Dye3** (1.38 x 10^{17} molecule cm^{-2}) is significantly less than **Dye2** (4.55 x 10^{17} molecule cm^{-2}). Finally, **Dye3** with extra-bulky donor exhibits poorer energy conversion efficiency of 3.91% compared to 5.45% of **Dye2,** under simulated AM 1.5 irradiation (100 mW cm^{-2}).

***Keywords*:** Dye-sensitized solar cells (DSCs), Density functional theory (DFT), N-substituted donors, Molecular volume, Molecular width, Dye uptake, Number density effect

1. Introduction

Dye-sensitized solar cells (DSCs) have attracted great attention over the last 15 years owing to their prospect of high energy conversion efficiency and low production cost.[1, 2] The typical basic configuration is as follows: The mesoporous oxide layer, which is composed of a network of TiO_2 nanoparticles that have been sintered together to establish electronic conduction, is deposited on a transparent conducting oxide (TCO), on a glass or plastic substrate. The most commonly used substrate is glass coated with fluorine-doped tin oxide (FTO). Attached to the surface of the nanocrystalline film is a monolayer of the charge-transfer dye. Photoexcitation of the charge-transfer dye results in the injection of an electron into the conduction band of TiO_2, leaving the dye in its oxidized state. The dye is restored to its ground state by electron transfer from the electrolyte, which is usually an organic solvent containing the iodide/ triiodide redox system. The regeneration of the sensitizer by iodide, intercepts the recapture of the conduction-band-electron by the oxidized dye.[3] The basic electron transfer processes in DSCs are shown in **Figure 1.** Process 1 is the excitation of the dye electron from ground state to excited state. Process 2 is the injection of an electron into the conduction band of the semiconductor (TiO_2). Process 3 is when the electron flows through the outer electrical circuit. Process 4 occurs at the counter electrode where the electron is transferred to the electrolyte iodide/triiodide. Process 5 is the regeneration of the oxidized dye within the electrolyte system.

There are mainly three kinds of dyes commonly used in DSCs, including ruthenium dyes,[4] porphyrin dyes[5-9] and metal-free organic dyes.[10-15] Compared with the other two dye types, the metal-free organic D-π-A dyes have received a great deal of attention due to their low cost, relatively simple synthetic procedure, ease of molecular modification and tailoring, high molar extinction coefficients, and environmental friendliness.[16-18]

However, organic dyes also have their own drawbacks, such as a narrower absorption spectrum, and a faster charge recombination. In this study, we are attempting to improve their solar-to-electrical-energy conversion efficiency in DSCs regarding charge recombination. There are two different improper recombination types in DSCs. One is the "inner-path recombination" consisting of the recombination of an electron injected into the semiconductor with the dye action before dye regeneration, which deteriorates the rate of electron injection, leading to a decrease of photocurrent and J_{sc} value. The other type of charge recombination in DSCs is "outer-path recombination", which occurs between the injected electrons in the semiconducting oxide electrode and the oxidized electrolyte. It strongly affects the theoretical potential difference between the oxide electrode and the electrolyte, resulting in a reduced V_{oc}. One of the common strategies to suppress this improper recombination path, while also suppressing undesirable molecular aggregation, is to introduce a starburst-triarylamine derivative as a donor group in D-π-A dyes. An extra-bulky donor could prevent the electrolyte from approaching the surface of the semiconducting oxide electrode, therefore, J_{sc} and V_{oc} would be enhanced and finally provide better device performance.[19, 20] However, one drawback of this dye design is that its bulky donor greatly reduces the number density of the adsorbed dyes on the oxide electrode surface, which decreases the absolute amount of injected electrons from the dyes to the electrode, resulting in poorer photocurrent generation in DSCs.

Recently, various kinds of metal-free organic dyes have been developed as sensitizers in DSCs, and their efficiency has been improved gradually through molecular design. Many efficient organic dyes for DSCs containing triphenylamine,[21, 22] coumarin,[23, 24] indoline,[25] fluorene,[26] or carbazole [27] moieties have been developed, yielding efficiencies in the range of 4-9 %.[28] Among them, N-Substituted derivative dyes are promising due to the high efficiency and good stability.[15, 29]

In this study, molecular design concepts were introduced in order to additionally improve their solar-to-electrical-energy conversion efficiency in DSCs regarding electron injection efficiency. We are attempting to disclose the relationship between the performance, structures, and the number density of the adsorbed dye on the TiO_2 surface using combined theoretical and experimental investigations of the physical properties of dye sensitizers. The effect of different N-Substituted electron donating[30-32] has been investigated. The calculated results are very helpful when designing and synthesising novel dye sensitizers with higher performance.[11-13]

2. Computational details

The ground-state structures of organic dye molecules are fully optimized using density functional theory (DFT) at the Becke3 (exchange) and the Lee-Yang-Parr (correlation) hybrid functional[33] with 6-31G (d,p) basis set.[34] The excitation energies and the electronic absorption spectra of organic dye molecules are investigated using time-dependent density functional theory (TDDFT) at the CAM-B3LYP functional,[35] with the same basis set as in the ground-state calculations. The solvation effect is included by means of conductor-like polarizable continuum model (C-PCM). The solvent used in our calculations and experiment is dichloromethane (CH_2Cl_2). The absorption spectra of all organic sensitizers and the contribution of molecular orbitals in the electronic transitions are simulated using the GaussSum program version 3.0.[36] The results are compared with the experimental data.[37] All calculations are performed using the Gaussian09 program package.[38]

The electron-injection characteristics from **Dye2** and **Dye3** to the TiO_2 (101) anatase surface[11] are carried out. The dye@$(TiO_2)_{38}$ systems are fully optimized by the Perdew-Burke-Ernzerhof (PBE) functional with the double numerical polarization (DNP) basis set. The core electron is treated with DFT-semicore Pseudopotentials (DSPPs) by DMol^3 code in Materials Studio 7.0^{TM}. The energy convergence tolerance is set to 2 x10^{-5} Ha, the maximum

force 0.004 Ha/Å, and the maximum displacement 0.005 Å. The optical properties of the relaxed complex are then computed with the TD-CAM-B3LYP/6-31G(d) method.

The adsorption energies (E_{ads}) of dyes on the $(TiO_2)_{38}$ clusters can be obtained using the following expression:

$$E_{ads} = E_{dye+TiO_2} - [E_{dye} + E_{TiO_2}]$$

where $E_{dye+TiO_2}$ is the total energy of the dye@$(TiO_2)_{38}$ system, and E_{dye} and E_{TiO_2} are the energies of the dye and $(TiO_2)_{38}$ cluster, respectively. Negative value indicates stable adsorption.

3. Results and discussion

The derivatives of N-substituted donor with D-π-A architecture in the present study, namely **Dye1**, **Dye2,** and **Dye3** are theoretically investigated. These dyes compose of an electron-accepting cyanoacrylic acid group (A) and a π-conjugated bridge (π) of one thiophene moiety while there are different electrons donating moieties on the donor group (D). We aim to reveal the effects of the sensitizer donor on the performance of the photovoltaic devices affecting both the geometrical structures and the optical properties of the derivatives of N-substituted donor with a D-π-A structure. Therefore, the introductions of more electron donors on a simple D-π-A dye system are designed, as can be seen in **Figure 2**. The variations of the donor are categorized into two types: (i) carbazole substituted at N-position (ii) Diphenylamine (DPA)-like substituted at N- position, one phenyl of DPA is replaced by naphthalene unit forming **Dye2** while in **Dye3**, two phenyl units of DPA are replaced by naphthalene and fluorene, respectively. **Figure 2** shows the molecular structures of **Dye1-3** which are studied for the purpose of comparing the variation and architecture of the donor.

3.1 Ground-state geometries of organic sensitizers

The optimized geometries obtained by density functional theory (DFT) B3LYP/6-31G(d,p) level of organic dye molecules are shown in **Figure 3,** and selected important inter-ring distance and dihedral angle parameters are listed in **Table 1.** The bond lengths of all the important inter-ring bonds are in the range of 1.40 to 1.46 Å. Due to the rigid structural arrangement of a carbazole donor, the dihedral angles between the donor unit (**D**) and the Phenyl ring (**Ph**) is calculated to be 49.27º which is significantly larger than those of **Dye2** and **Dye3** (26.71º and 26.86º), with free rotation around the N- position of a DPA-like structure. Consequently, the twisted structure in the donor part of these dyes resulted in preventing dye aggregation.[39, 40] In the acceptor part, the dihedral angles between the Thiophene ring (**T**) and the Cyanoacrylic acid anchoring are coplanar in the range of 0.64º to 1.08º. Therefore, the electron from the donor can efficiently delocalize to the acceptor moiety and as a result transfers to the conduction band (CB) of the semiconductor.

3.2 Electronic structures of organic sensitizers

To gain insight into the electronic structures, frontier molecular orbitals are obtained to examine the highest occupied molecular orbital (HOMO) and the lowest unoccupied molecular orbital (LUMO) due to the relative ordering of the HOMO and LUMO which provides a reasonable qualitative indication of the charge transfer properties. The molecular orbitals of **Dye1**, **Dye2**, and **Dye3** are depicted in **Figure 4** and the density of state (DOS) are presented in **Table 2.** In organic sensitizers, the electron density on the HOMO is delocalized on donor group and the electron density on the LUMO is delocalized on acceptor group. The HOMO to LUMO transition corresponds to the intramolecular charge transfers (ICT) from the donor group to the acceptor group. The different electronic densities between the ground state and excited state (shown in **Figure 4**) are clearly assigned to the unambiguous character of excited state. Obviously, the decreasing electron density is primarily from the electron

donor, whereas the increasing electron density is mainly on the acceptor group, which is indicative of the intramolecular charge transfer when transition occurs upon photo-irradiation. This agrees well with the electronic structure analysis discussed above. Moreover, the HOMO of all dyes show that the electrons density of **Dye1** is predominantly located at the rigid carbazole moiety while in **Dye2** and **Dye3**, the electron is located all over the donor moiety and contributed to the linker part. Therefore intramolecular charge transfer could be more efficient in **Dye2** and **Dye3** than in **Dye1** according to Marcus theory. The distance of charge transfer (D_{CT}, Å) and the transition dipole moment (μ, Debye) are calculated for a better understanding of the performance of the intramolecular charge transfer upon photoexcitation. The D_{CT} is the spatial distance between two barycenters of the density depletion (ρ-) and density enhancement (ρ+) distributions, while dye is under irradiation.[41] The isosurface (ρ-/ρ+) of the dyes are illustrated in **Figure 5,** and the D_{CT} and μ values are listed in **Table 3**. As shown, the D_{CT} values (Å) are found to be in this order: **Dye1** (3.59) < **Dye2** (4.04) < **Dye3** (4.20). The μ also give the same trend as **Dye1** (12.9) < **Dye2** (14.9) < **Dye3** (15.9). Based on the D_{CT} and μ, **Dye3** is predicted to give the best DSC performance among these dyes.

In addition, suitable energy levels of the HOMO and the LUMO orbitals of the organic dye are required to match the I^-/I_3^- redox potential and conduction band level of the TiO_2 semiconductor. The calculated molecular orbital energies of **Dye1-3** are computed by using B3LYP/6-31G(d,p) in CH_2Cl_2 as shown in **Figure 6.** For the LUMO levels, the results show that the replacement of carbazole with diphenylamine-like substituent raises the the LUMO level from -2.80 **(Dye1)** to -2.69 eV **(Dye2** and **Dye3)**. However, the LUMO levels of all dyes lie above the E_{CB} of TiO_2 leading to efficient injection of excited electrons into the semiconductor electrode. Compared with electrolyte redox potential, the HOMO levels of all dyes are below the I^-/I_3^- redox potential. These results show the accepting electron efficiency

of the oxidized dye from the electrolyte system. The HOMO energy levels of **Dye1**, **Dye2,** and **Dye3** are calculated to be -5.37, -5.22, and -5.12 eV, respectively. As shown, the HOMO levels of **Dye1-3** are systematically increased with increasing donor ability (**Dye3** < **Dye2** < **Dye1**) approaching the redox potential of the electrolyte system, which resulted in the energy gaps being in a sequence of **Dye3** (2.43) < **Dye2** (2.53 eV) < **Dye1 (**2.57 eV). Therefore, **Dye3** with its narrow energy gap would be an efficient sensitizer to extend the absorption wavelengths of these organic dyes.

3.3 Absorption spectra of organic sensitizers

The absorption spectra of these molecules have been studied by TD-CAM-B3LYP/6-31G(d,p) level in the CH_2Cl_2 solvent. Comparison of the theoretically calculated wavelength with experimental data[37] has been performed. The corresponding simulated absorption spectra of **Dye1-3** are shown in **Figure 7.** The electronic properties, oscillator strengths, configurations of the orbitals, and the maximum wavelength in the solvent phase of all organic sensitizers are shown in **Table 3.** The strongest absorption peak with the largest oscillator strength arises from $S_0 \rightarrow S_1$ transition and corresponds to the intramolecular charge transfer transition, which is primarily contributed from the HOMO to the LUMO. It is found that the calculated data have similar tendencies with the experiment. The trend of maximum absorption wavelength is **Dye3** > **Dye2** > **Dye1** which exhibits red-shift and the absorption intensity increases with the increase of electron donating ability of donor groups. This tendency also confirms the D_{CT} prediction. These results indicate that **Dye1** exhibits obvious blue-shift due to the electrons from the rigid carbazole donor, connected at N-position with large twisted angle, hardly transferred to the anchoring group. Therefore, its conjugation length, and D_{CT} values are smallest in comparison to **Dye2** and **Dye3**. In the next section, the adsorption of the organic sensitizers on the TiO_2 cluster, of **Dye2** and **Dye3** will be compared and discussed.

3.4 Adsorption of organic sensitizers on the TiO_2 cluster

The TiO_2 film were modelled with a stoichiometric anatase (101) surface as the $(TiO_2)_{38}$ cluster, which is similar to that described by Nazeeruddin et al.[42] This model has been wildly used to study dye@TiO_2 adsorption and represents a reasonable choice between accuracy and computational convenience, and nicely reproduces the main electronic characteristics of TiO_2 nanoparticles.[8, 10-14, 43-45] The HOMO, LUMO and HOMO–LUMO energy gap of the this cluster are calculated to be 27.98, 23.52, and 24.46 eV, respectively, while the lowest excitation is obtained as 3.75 eV[45] which is reasonably higher than typical band gaps of TiO_2 nanoparticles of a few nm size of 3.2–3.3 eV.[46, 47] The TiO_2 conduction band edge was calculated at ca. -4 eV vs. vacuum, in good agreement with experimental values.[48] In addition, this cluster size has been comparatively tested with a relatively larger $(TiO_2)_{82}$ cluster and the both clusters shows a similar conduction band structure, within 0.1 eV, to the corresponding periodic model.[49] Therefore, this work we use the $(TiO_2)_{38}$ cluster for representing the TiO_2 surface for dye adsorption.

The optimized structures of dye@(TiO2)38 adsorption complexes are shown in **Figure 8**. The intermolecular Ti–O bond distances and adsorption energies calculated by PBE/DNP are tabulated in **Table 5**. The bond distances between 5c-Ti and O atom of **Dye2** and **Dye**3 are in range of 2.140–2.262 Å. The adsorption energy (E_{ads}) of **Dye2**@TiO_2 and **Dye3**@TiO_2 are calculated to be -15.89 and -19.54 kcal/mol respectively, indicating the strong interactions between the dyes and the TiO_2 cluster. The higher adsorption energy of **Dye3,** with a stronger electron donating group, can be related to the stronger electronic coupling strengths between the anchoring group of dye and the TiO_2 surface, which could corresponds to higher observed J_{sc}. However, we found that the adsorption energies did not correspond to observed J_{sc} as expected. The J_{sc} of 10.96 mA cm^{-2} for **Dye2** is significantly higher than 7.62 mA cm^{-2} for **Dye3**. These results can be rationalized by molecular volume

and projected area **(Figure 9)**, as well as molecular width **(Figure 8)**. The molecular volume is calculated by a Connelly surface, which represents the molecular volume of the dye including its van der Waals volume. The projected area explains the area on the TiO_2 surface that is occupied by the adsorbed dye. These values of **Dye2** and **Dye3** are listed in **Table4**. As shown, the molecular widths are calculated to be 14.505 Å and 15.980 Å **(Figure 8)**, the molecular volumes are 1810.68 $Å^3$ and 1937.13 $Å^3$ **(Table 4)**, together with the measured projected area (dark area in **Figure 9**) of 180 $Å^2$ and 214 $Å^2$, for **Dye2** and **Dye3** respectively, which correspond to the dye uptakes of 4.55 x 10^{17} and 1.38 x 10^{17} molecule/cm^2, see **Table 4**. These results indicate that **Dye3** would cover a larger area on the TiO_2 surface due to the bulky of the donor moiety. Consequently, the number density of the adsorbed **Dye3** on the surface could be reduced leading to the lower dye uptake. Then the absolute amount of injected electrons from the dyes to the electrode per cm^2 is decreased, related to the lower observed J_{sc} value of 7.62 mA cm^{-2} compared to 10.96 mA cm^{-2} of **Dye2.** These findings highlight the poorer energy conversion efficiency of 3.91% in **Dye3** compared to the better performance of 5.45% in **Dye2** under simulated AM 1.5 irradiation (100 mW cm^{-2}), see **Table 5**.

3.5 Dye@TiO_2 adsorption and the electron injection mechanism

To study the electron injection mechanism of selected dyes at the interface of the dye@TiO_2 surface, the ten lowest vertical transitions are simulated using TD-CAM-B3LYP/6-31G(d).The calculated excitation energies for the peak having the highest oscillator strength are illustrated in **Figure 10.** The results show that the strongest transition in our dyes is characterized as a linear combination of some configurations. The Kohn-Sham orbitals, which are most relevant to these transitions, are shown in **Figure 11 (a)**, **(b)**. There is a very similar trend between **Dye2** and **Dye3**, Therefore we only discuss **Dye3**. The highest oscillator strength of 1.5635 for **Dye3** is assigned as the linear combination of

0.17(H→L+25) + 0.14(H-1→L+27) + 0.27(H-2→L+38). These orbitals, together with TDDFT functional, show that the transition with large oscillator strength is characterized as the transition from the orbitals localized in the donor-π-spacer (D–π) unit to the orbitals delocalized over the acceptor (A) unit of dyes and the $(TiO_2)_{38}$ cluster. The former orbitals are similar to the HOMOs of dyes and the latter orbitals correspond to the interacting orbitals between the LUMOs of dyes and the conduction band of TiO_2. This means that the electron excitation of this system directly induces the electron injection from dye into TiO_2 surface. This is the origin of the high photoelectric conversion efficiency of this system. Note that the latter orbitals are firstly embedded in the conduction band of TiO_2 and then the injected electron is transferred to the conduction bands of TiO_2. These compositions of the electronic transitions for two dyes, as shown in **Figure 11(a)**, **(b)**, strongly indicated that when the intramolecular charge transfer is initially performed, electrons moved from the donor to the anchoring group via phenyl-thiophene bridging, then jumped onto the TiO_2 surface.

4. Conclusions

In summary, **Dye1, Dye2 and Dye3** have been studied for the purpose of comparison, based on the variation and architecture of the donor, N-substituted donors-π-acceptor type. These dyes are composed of cyanoacrylic acid anchoring group and phenyl-thiophene moiety as π-specer. We have designed 3 different donors for variation, carbazole substituted at N-position forming **Dye1**, Diphenylamine (DPA)-like substituted at N- position, one phenyl of DPA is replaced by naphthalene unit forming **Dye2**, while two phenyl units of DPA are replaced by naphthalene and fluorene forming **Dye3**, respectively. We found that **Dye3**, with the strongest electron donating ability, shows the most red shift in the UV absorption spectra and the highest performance charge transfer. Moreover, the calculated adsorption energy -19.54 kcal/mol for Dye3@$(TiO_2)_{38}$ complex indicates the strongest interactions between the dyes and the TiO_2 surface, therefore **Dye3** is expected to be the most potential sensitizer.

Nevertheless, **Dye2** has shown the best photovoltaic performance. This controversial issue has been solved by performing the molecular volume, projected area on the TiO_2 surface and molecular width to investigate the effect of N-substituted donors on the number density of the adsorbed dye on TiO_2 surface. It has been found that the more bulky donor moiety in **Dye3** reduces the number density of the adsorbed dye on the TiO_2 surface. The molecular width of **Dye2** and **Dye3** are calculated to be 14.505 Å and 15.980 Å together with the computed projected area of 180 and 214 $Å^2$ (**Figure 8**) which excellently agrees with the dye uptake of 4.55×10^{17} and 1.38×10^{17} molecule/cm^2, respectively. The photovoltaic performance shows a poorer energy conversion efficiency of 3.91% in **Dye3** compared to the significantly better performance of 5.45% in **Dye2** under simulated AM 1.5 irradiation (100 mW cm^{-2}). In conclusion, it has been shown that these computational tools described above can provide detailed characterizations, which can qualitatively explain experimental efficiency and therefore can be of great valuable in further design of novel organic sensitizers for higher efficiency photovoltaic devices.

5. Acknowledgements

The authors would like to acknowledge the Department of Chemistry, Faculty of Science, Ubon Ratchathani and Chiang Mai University including the National Nanotectology Center (NANOTEC) for using their computer resources. The work is financially supported by the Thailand Graduate Institute of Science and Technology (TGIST) (No. TGIST 01-57-042), Thailand Research Fund (grant number RSA5780048) and the Center of Excellence for Innovation in Chemistry (PERCH-CIC), Office of the Higher Education Commission, Ministry of Education are gratefully acknowledged.

References

1. B. O'Regan, Gratzel, Michael, *Nature* 1991, **353**, 737-740.
2. B.-G. Kim, K. Chung and J. Kim, *Chemistry – A European Journal*, 2013, **19**, 5220-5230.
3. A. Hagfeldt, G. Boschloo, L. Sun, L. Kloo and H. Pettersson, *Chemical Reviews*, 2010, **110**, 6595-6663.
4. B. Peña, A. David, C. Pavani, M. S. Baptista, J.-P. Pellois, C. Turro and K. R. Dunbar, *Organometallics*, 2014, **33**, 1100-1103.
5. W. M. Campbell, K. W. Jolley, P. Wagner, K. Wagner, P. J. Walsh, K. C. Gordon, L. Schmidt-Mende, M. K. Nazeeruddin, Q. Wang, M. Grätzel and D. L. Officer, *The Journal of Physical Chemistry C*, 2007, **111**, 11760-11762.
6. A. S. Hart, C. B. Kc, H. B. Gobeze, L. R. Sequeira and F. D'Souza, *ACS Applied Materials & Interfaces*, 2013, **5**, 5314-5323.
7. S. Karthikeyan and J. Y. Lee, *The Journal of Physical Chemistry A*, 2013, **117**, 10973-10979.
8. S. Namuangruk, K. Sirithip, R. Rattanatwan, T. Keawin, N. Kungwan, T. Sudyodsuk, V. Promarak, Y. Surakhot and S. Jungsuttiwong, *Dalton Transactions*, 2014, **43**, 9166-9176.
9. T. Ripolles-Sanchis, B.-C. Guo, H.-P. Wu, T.-Y. Pan, H.-W. Lee, S. R. Raga, F. Fabregat-Santiago, J. Bisquert, C.-Y. Yeh and E. W.-G. Diau, *Chemical Communications*, 2012, **48**, 4368-4370.
10. S. Jungsuttiwong, T. Yakhanthip, Y. Surakhot, J. Khunchalee, T. Sudyoadsuk, V. Promarak, N. Kungwan and S. Namuangruk, *Journal of Computational Chemistry*, 2012, **33**, 1517-1523.
11. S. Namuangruk, R. Fukuda, M. Ehara, J. Meeprasert, T. Khanasa, S. Morada, T. Kaewin, S. Jungsuttiwong, T. Sudyoadsuk and V. Promarak, *The Journal of Physical Chemistry C*, 2012, **116**, 25653-25663.
12. S. Namuangruk, J. Meeprasert, S. Jungsuttiwong, V. Promarak and N. Kungwan, *Theoretical Chemistry Accounts*, 2014, **133**, 1-15.
13. R. Tarsang, V. Promarak, T. Sudyoadsuk, S. Namuangruk and S. Jungsuttiwong, *Journal of Photochemistry and Photobiology A: Chemistry*, 2014, **273**, 8-16.
14. R. Tarsang, V. Promarak, T. Sudyoadsuk, S. Namuangruk, N. Kungwan and S. Jungsuttiwong, *ChemPhysChem*, 2014, n/a-n/a.
15. P. Thongkasee, A. Thangthong, N. Janthasing, T. Sudyoadsuk, S. Namuangruk, T. Keawin, S. Jungsuttiwong and V. Promarak, *ACS Applied Materials & Interfaces*, 2014, **6**, 8212-8222.
16. Z. Chen, F. Li and C. Huang, *Current Organic Chemistry*, 2007, **11**, 1241-1258.
17. A. Dualeh, F. De Angelis, S. Fantacci, T. Moehl, C. Yi, F. Kessler, E. Baranoff, M. K. Nazeeruddin and M. Grätzel, *The Journal of Physical Chemistry C*, 2011, **116**, 1572-1578.
18. X. Ren, S. Jiang, M. Cha, G. Zhou and Z.-S. Wang, *Chemistry of Materials*, 2012, **24**, 3493-3499.
19. J. Tang, J. Hua, W. Wu, J. Li, Z. Jin, Y. Long and H. Tian, *Energy & Environmental Science*, 2010, **3**, 1736-1745.
20. Z. Ning and H. Tian, *Chemical Communications*, 2009, 5483-5495.
21. M. Liang, W. Xu, F. Cai, P. Chen, B. Peng, J. Chen and Z. Li, *The Journal of Physical Chemistry C*, 2007, **111**, 4465-4472.
22. H. Tian, X. Yang, R. Chen, R. Zhang, A. Hagfeldt and L. Sun, *The Journal of Physical Chemistry C*, 2008, **112**, 11023-11033.

23. K. Hara, Z.-S. Wang, T. Sato, A. Furube, R. Katoh, H. Sugihara, Y. Dan-oh, C. Kasada, A. Shinpo and S. Suga, *The Journal of Physical Chemistry B*, 2005, **109**, 15476-15482.
24. Z. S. Wang, Y. Cui, K. Hara, Y. Dan-oh, C. Kasada and A. Shinpo, *Advanced Materials*, 2007, **19**, 1138-1141.
25. T. Horiuchi, H. Miura, K. Sumioka and S. Uchida, *Journal of the American Chemical Society*, 2004, **126**, 12218-12219.
26. C.-H. Chen, Y.-C. Hsu, H.-H. Chou, K. R. J. Thomas, J. T. Lin and C.-P. Hsu, *Chemistry – A European Journal*, 2010, **16**, 3184-3193.
27. Z.-S. Wang, N. Koumura, Y. Cui, M. Takahashi, H. Sekiguchi, A. Mori, T. Kubo, A. Furube and K. Hara, *Chemistry of Materials*, 2008, **20**, 3993-4003.
28. B.-G. Kim, C.-G. Zhen, E. J. Jeong, J. Kieffer and J. Kim, *Advanced Functional Materials*, 2012, **22**, 1606-1612.
29. L. Liu, X. Meng, W. Li, X. Zhou, Z. Bai, D. Liu, Y. Lv and R.-h. Li, *Dyes and Pigments*, 2014, **108**, 32-40.
30. Y. J. Chang and T. J. Chow, *Tetrahedron*, 2009, **65**, 4726-4734.
31. Z. Wan, C. Jia, L. Zhou, W. Huo, X. Yao and Y. Shi, *Dyes and Pigments*, 2012, **95**, 41-46.
32. P. Surawatanawong, A. K. Wójcik and S. Kiatisevi, *Journal of Photochemistry and Photobiology A: Chemistry*, 2013, **253**, 62-71.
33. A. D. Becke, *The Journal of Chemical Physics*, 1993, **98**, 1372-1377.
34. M. M. Francl, W. J. Pietro, W. J. Hehre, J. S. Binkley, D. J. DeFrees, J. A. Pople and M. S. Gordon, *The Journal of Chemical Physics*, 1982, **77**, 3654 − 3666.
35. T. Yanai, D. P. Tew and N. C. Handy, *Chemical Physics Letters*, 2004, **393**, 51-57.
36. N. M. O'boyle, A. L. Tenderholt and K. M. Langner, *Journal of Computational Chemistry*, 2008, **29(5)**, 839-845.
37. K. Ronyhut, Senior project submitted in "Fabrication and characterization of dye sensited solar cell based (Z)-2-cyano-3-(5-(4-(naphthalene-2-ylamino)phenyl)thiophen-2-yl)acrylic acid" Department of chemistry, for the degree of B. Sc. in Chemistry Faculty of Science Ubon Ratchathani University, 2013 edn.,

.
38. M. J. T. Frisch, G. W.; Schlegel, H. B.; Scuseria, G. E.; Robb, M. A.; Cheeseman, J. R.; Scalmani, G.; Barone, V.; Mennucci, B.; Petersson, G. A.; Nakatsuji, H.; Caricato, M.; Li, X.; Hratchian, H. P.; Izmaylov, A. F.; Bloino, J.; Zheng, G.; Sonnenberg, J. L.; Hada, M.; Ehara, M.; Toyota, K.; Fukuda, R.; Hasegawa, J.; Ishida, M.; Nakajima, T.; Honda, Y.; Kitao, O.; Nakai, H.; Vreven, T.; Montgomery, J. A.; Jr.; Peralta, J. E.; Ogliaro, F.; Bearpark, M.; Heyd, J. J.; Brothers, E.; Kudin, K. N.; Staroverov, V. N.; Kobayashi, R.; Normand, J.; Raghavachari, K.; Rendell, A.; Burant, J. C.; Iyengar, S. S.; Tomasi, J.; Cossi, M.; Rega, N.; Millam, J. M.; Klene, M.; Knox, J. E.; Cross, J. B.; Bakken, V.; Adamo, C.; Jaramillo, J.; Gomperts, R.; Stratmann, R. E.; Yazyev, O.; Austin, A. J.; Cammi, R.; Pomelli, C.; Ochterski, J. W.; Martin, R. L.; Morokuma, K.; Zakrzewski, V. G.; Voth, G. A.; Salvador, P.; Dannenberg, J. J.; Dapprich, S.; Daniels, A. D.; Farkas, O.; Foresman, J. B.; Ortiz, J. V.; Cioslowski, J.; Fox, D. J., , 2009., **Gaussian 09, Revision C.01, Gaussian, Inc., Wallingford CT**.
39. C. Jia, Z. Wan, J. Zhang, Z. Li, X. Yao and Y. Shi, *Spectrochimica Acta Part A: Molecular and Biomolecular Spectroscopy*, 2012, **86**, 387-391.
40. X. Chen, C. Jia, Z. Wan, J. Zhang and X. Yao, *Spectrochimica Acta Part A: Molecular and Biomolecular Spectroscopy*, 2014, **123**, 282-289.
41. T. Le Bahers, C. Adamo and I. Ciofini, *Journal of Chemical Theory and Computation*, 2011, **7**, 2498-2506.

42. M. K. Nazeeruddin, F. De Angelis, S. Fantacci, A. Selloni, G. Viscardi, P. Liska, S. Ito, T. Bessho and M. Gratzel, *Journal of the American Chemical Society*, 2005, **127**, 16835-16847.
43. S. Jungsuttiwong, R. Tarsang, T. Sudyoadsuk, V. Promarak, P. Khongpracha and S. Namuangruk, *Organic Electronics*, 2013, **14**, 711-722.
44. E. Ronca, M. Pastore, L. Belpassi, F. Tarantelli and F. De Angelis, *Energy & Environmental Science*, 2013, **6**, 183-193.
45. T. Yakhanthip, S. Jungsuttiwong, S. Namuangruk, N. Kungwan, V. Promarak, T. Sudyoadsuk and P. Kochpradist, *Journal of Computational Chemistry*, 2011, **32**, 1568-1576.
46. M. Khoudiakov, A. R. Parise and B. S. Brunschwig, *J. Am. Chem. Soc.*, 2003, **125**, 4637–4642.
47. Y.-X. Weng, Y.-Q. Wang, J. B. Asbury, H. N. Ghosh and T. Lian, *Journal of Physical Chem. B*, 2000, **104**, 93–104.
48. F. De Angelis, S. Fantacci and A. Selloni, *Nanotechnology*, 2008, **19**, 424002.
49. F. De Angelis, S. Fantacci, E. Mosconi, M. K. Nazeeruddin and M. Graetzel, *Journal of Physical Chemistry C*, 2011, **115**, 8825-8831.

Figure Captions

Figure 1 Working principle of a typical DSC.

Figure 2 Sketch map of the synthesized **Dye1**, **Dye2** and **Dye3** sensitizer.

Figure 3 Optimized structures of **Dye1** and **Dye2** by DFT/B3LYP/6-31G (d,p).

Figure 4 HOMO (left) LUMO (middle) and charge density difference (right) between the excited and ground states of the dyes. The green and red colors indicate a decrease and increase of charge density.

Figure 5 ρ-/ρ+ (green/ red) isocontour surfaces of (a) **Dye1**, (b) **Dye2**, and (c) **Dye3**, computed at the TD-CAM-B3LYP level.

Figure 6 Molecular orbital energy level diagram of the dyes, TiO_2 conduction band, and redox potential of I^-/I_3^- electrolyte.

Figure 7 Absorption spectra of **Dye1**, **Dye2** and **Dye3** calculated by TD-CAM-B3LYP/6-31G (d,p) level in CH_2Cl_2 solvent (C-PCM model).

Figure 8 Molecular widths of **Dye2** and **Dye3** calculated by PBE/DNP on DMol^3 program.

Figure 9 Molecular volume and projected area of **Dye2** and **Dye3**.

Figure 10 Absorption spectra of **Dye2@TiO_2** and **Dye3@TiO_2** calculated by TD-CAM-B3LYP/6-31G(d) level in gas phase.

Figure 11 MOs relevant to the transition from S0 to S1 of organic sensitizer adsorbed on the $(TiO_2)_{38}$ in gas phase calculated by TD-CAM-B3LYP/6-31G(d) on DMol^3 geometry. (a) **Dye2@TiO_2** (b) **Dye3@TiO_2**.

Table 1

The selected important dihedral angles (Φ, °) and inter-ring distances (r, Å) in parenthesis calculated by B3LYP/6-31G(d,p) method.

Dyes	Dihedral angle and inter-ring distance		
	D - Ph	Ph -T	T - CA
Dye1	-49.27 (1.41)	23.75 (1.46)	-0.64 (1.42)
Dye2	-26.71 (1.40)	20.78 (1.45)	-1.05 (1.42)
Dye3	-26.86 (1.40)	21.02 (1.45)	1.08 (1.42)

D = Donor, Ph = Phenyl, T = Thiophene, CA = Cyanoacrylic acid

Table 2

The energies and percentage composition of frontier molecular orbitals of organic sensitizers

Dyes	Molecular orbitals	Orbitals energy (eV)	Percentage composition		
			Donor	Linker	Acceptor
Dye 1	LUMO	-2.80	2	49	49
	HOMO	-5.37	81	17	2
Dye 2	LUMO	-2.69	3	49	48
	HOMO	-5.22	47	44	9
Dye 3	LUMO	-2.69	3	49	48
	HOMO	-5.12	59	35	6

Table 3

The distance of charge transfer upon excitation (D_{CT}), dipole moment (μ) electronic properties, maximum absorption wavelength and oscillator strength (*f*) obtained by TDDFT at the CAM- B3LYP/6-31G (d,p) level of theory in CH_2Cl_2 solvent (C-PCM model).

Dyes	D_{CT} (Å)/ μ (Debye)	Electronic transitions	λ_{max} (nm/eV)	*f*	Assignment; H=HOMO, L=LUMO, etc.	Expt. [a] λ_{max} (nm/eV)
Dye1	3.59/12.9	$S_0 \rightarrow S_1$	397(3.12)	1.4218	(+0.53) H → L (+0.43) H-2 → L (-0.11) H → L+1	355/3.49
Dye2	4.04/14.9	$S_0 \rightarrow S_1$	428(2.90)	1.4686	(+0.62) H → L (+0.21) H-1 → L (-0.17) H-1 → L (-0.10) H → L+2	436/2.84
Dye3	4.20/15.6	$S_0 \rightarrow S_1$	434(2.85)	1.4867	(+0.60) H → L (+0.24) H-1 → L (-0.19) H-2 → L (-0.11) H → L+2	438/2.83

[a] experimental values are taken from [37]

Table 4

Molecular volume, box size, projected area and dye uptake of **Dye 2** and **Dye 3**.

Dyes	molecular volume[a] (Å^3)	Box size a x b x c (Å^3)	Projected area a x b (Å^2)	Dye uptake[b] (molecule cm^{-2})
Dye2	**1810.68**	**10 x 18 x 21.20**	**180**	**4.55 x 1017**
Dye3	**1937.13**	**10 x 21.40 x 21.20**	**214**	**1.38 x 1017**

[a] Molecular volume is calculated by Connolly surface.

[b] Experimental values are taken from [37].

Table 5

The selected bond length (Å) and adsorption energy (E_{ads}) of dye-TiO_2 calculated by PBE/DNP in DMol[3].

Dyes	Ti - O	Ti′ - O′	E_{ads} (kcal/mol)	J_{SC}[a] (mA cm^{-2})	V_{OC}[a] (V)	FF[a]	η[a] (%)
Dye2@TiO_2	2.140	2.262	-15.891	10.96	0.77	0.645	5.45
Dye3@TiO_2	2.142	2.180	-19.540	7.62	0.76	0.674	3.91

[a] Experimental values are taken from [37].

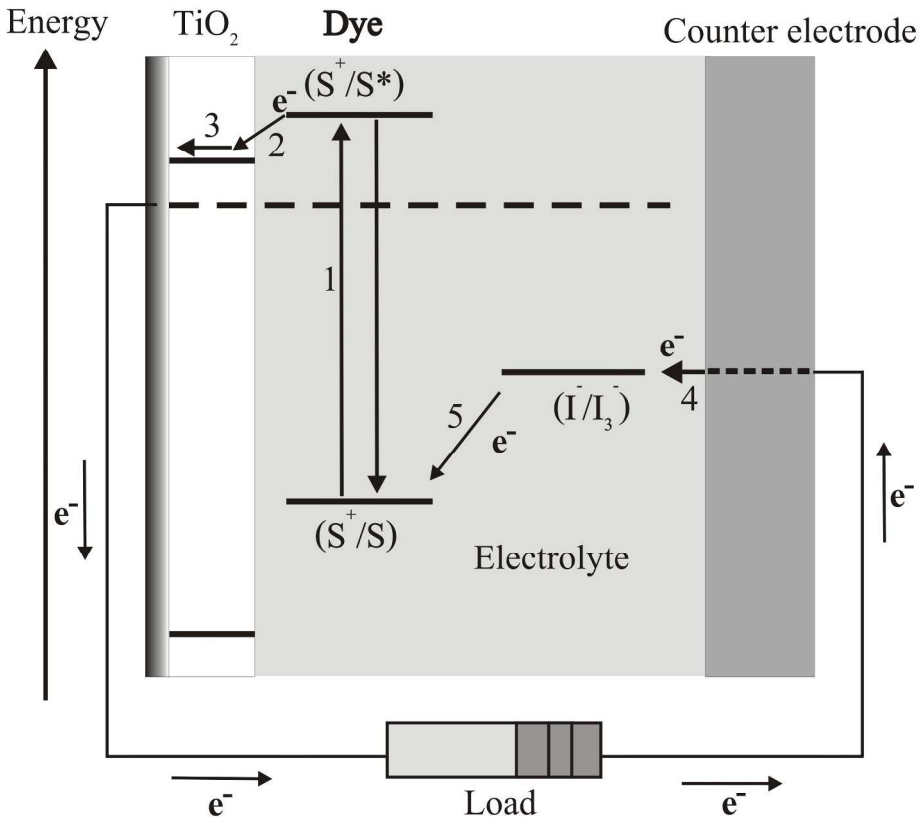

The basic electron transfer processes in DSCs.
236x213mm (300 x 300 DPI)

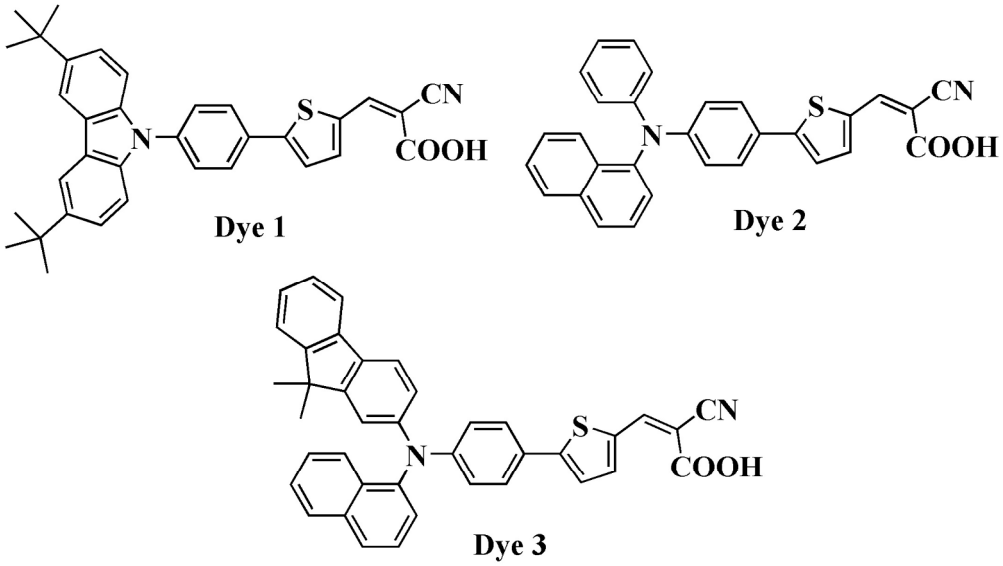

Sketch map of the synthesized Dye1, Dye2 and Dye3 sensitizer.
181x102mm (300 x 300 DPI)

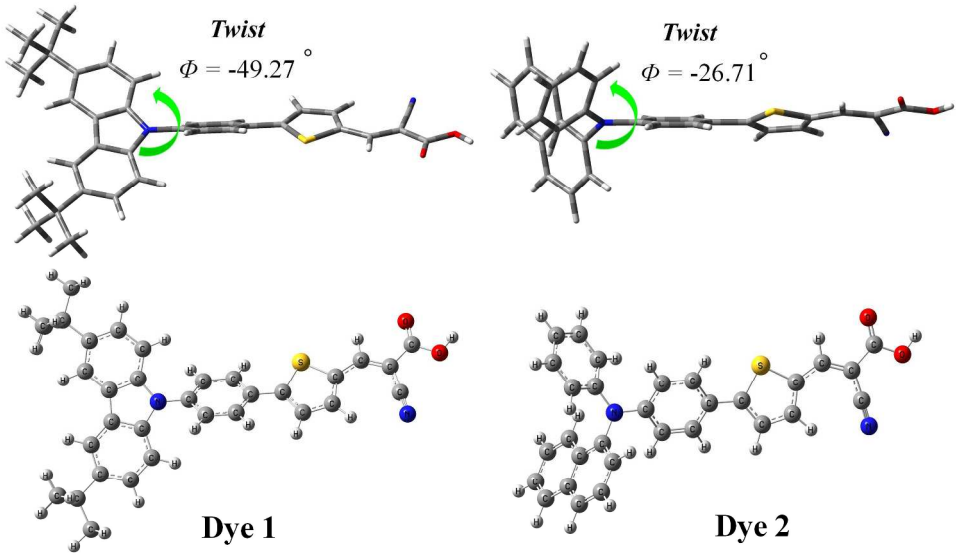

Optimized structures of Dye1 and Dye2 by DFT/B3LYP/6-31G (d,p).
1200x699mm (65 x 65 DPI)

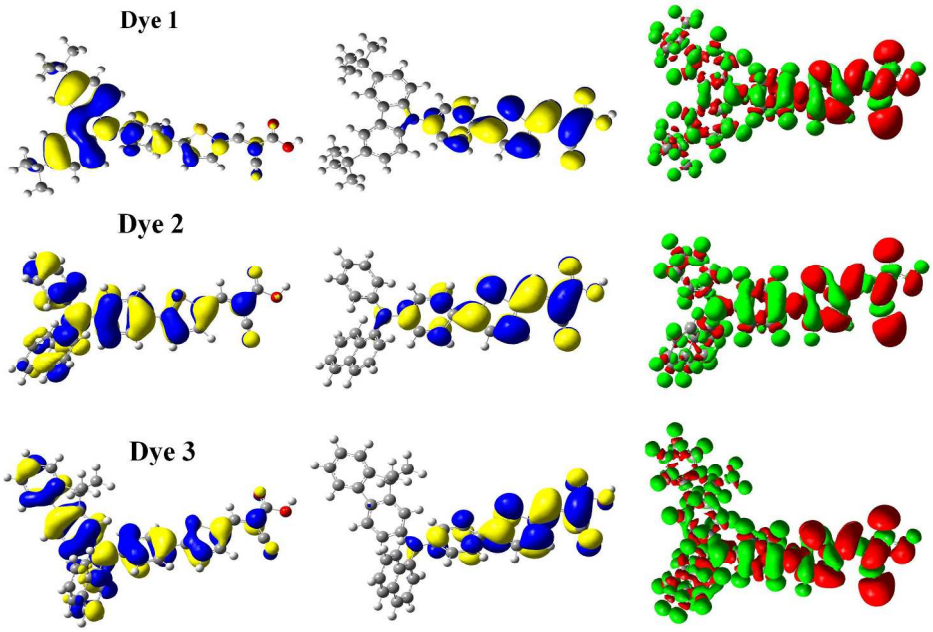

HOMO (left) LUMO (middle) and charge density difference (right) between the excited and ground states of the dyes. The green and red colors indicate a decrease and increase of charge density.
854x590mm (91 x 91 DPI)

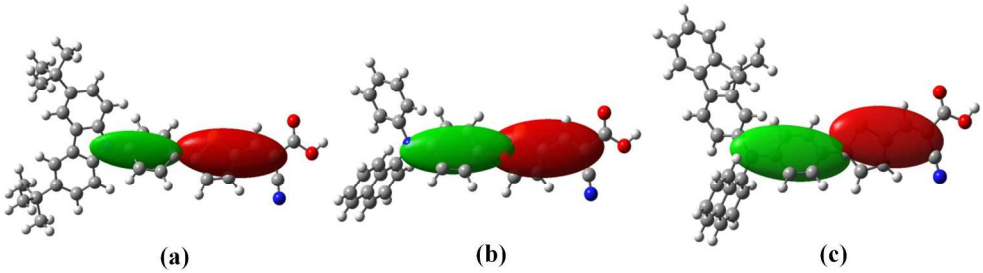

ρ-/ρ+ (green/ red) isocontour surfaces of (a) Dye1, (b) Dye2, and (c) Dye3, computed at the TD-CAM-B3LYP level.
750x350mm (96 x 96 DPI)

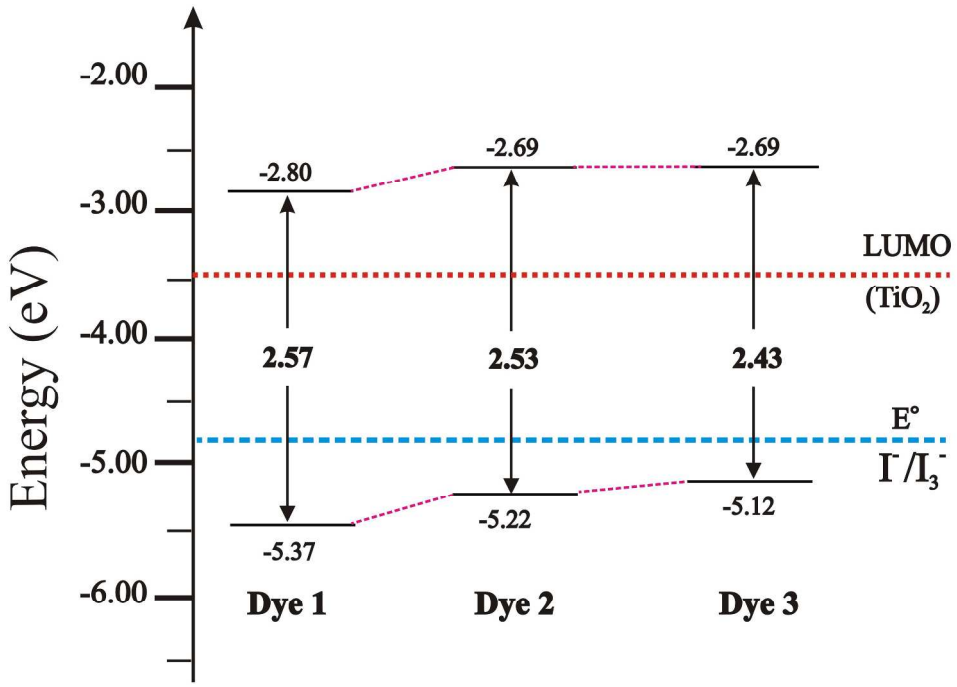

Molecular orbital energy level diagram of the dyes, TiO2 conduction band, and redox potential of I-/I3- electrolyte.
266x194mm (300 x 300 DPI)

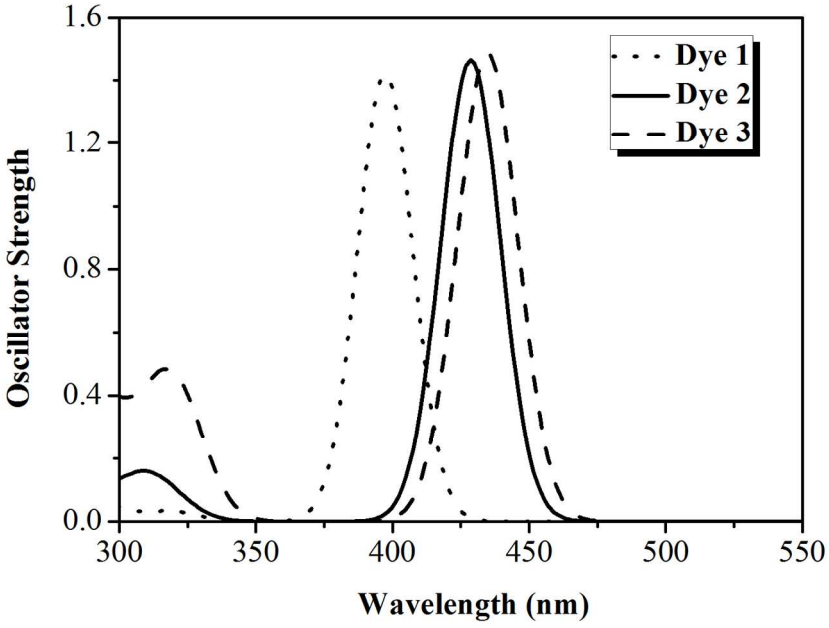

Absorption spectra of Dye1, Dye2 and Dye3 calculated by TD-CAM-B3LYP /6-31G (d,p) level in CH2Cl2 solvent (C-PCM model).
297x208mm (150 x 150 DPI)

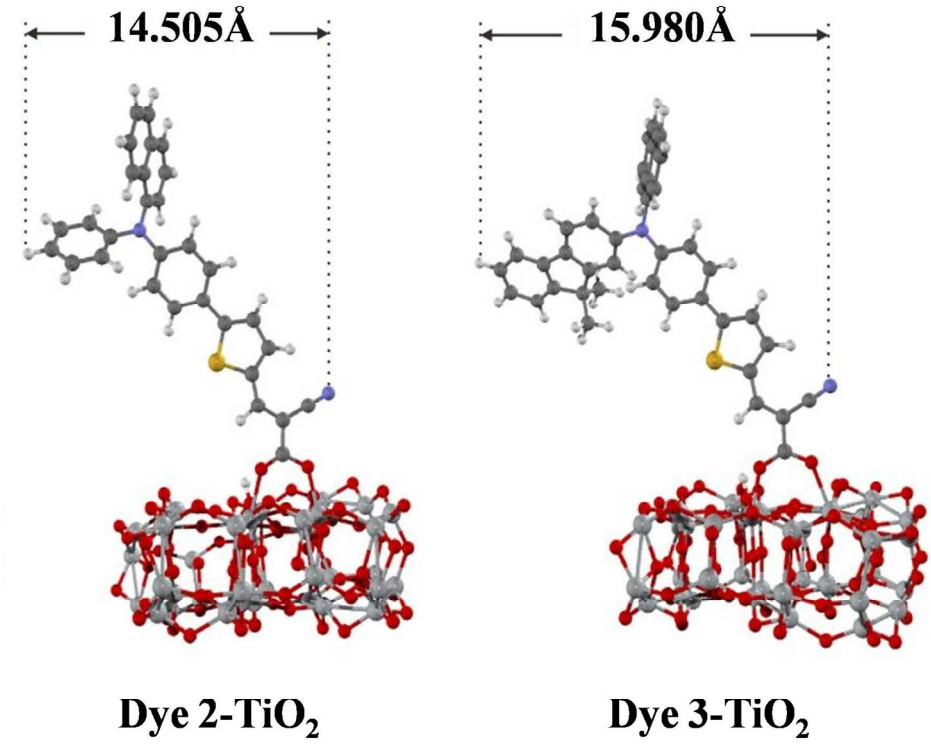

Molecular widths of Dye2 and Dye3 calculated by PBE/DNP on DMol3 program.
896x797mm (87 x 87 DPI)

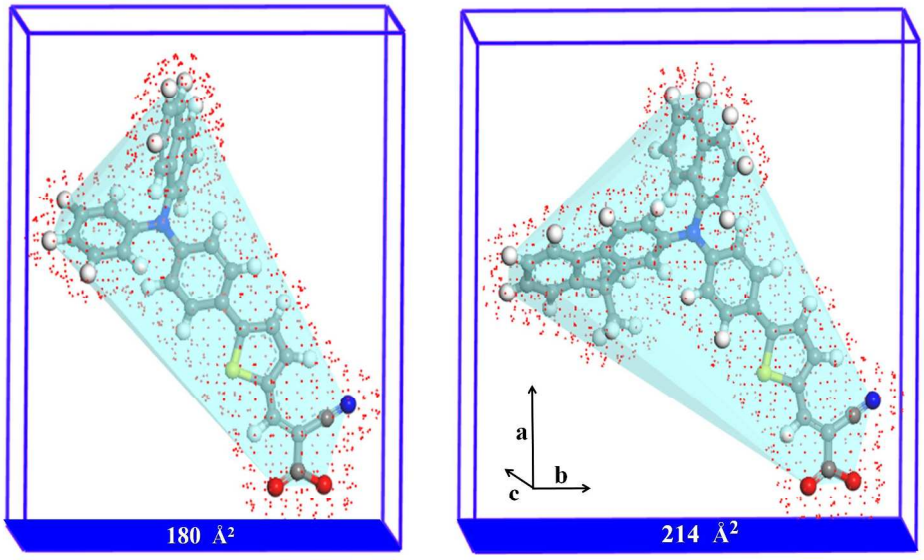

Dye 2 Dye 3

Molecular volume and projected area of Dye2 and Dye3.
1000x800mm (78 x 78 DPI)

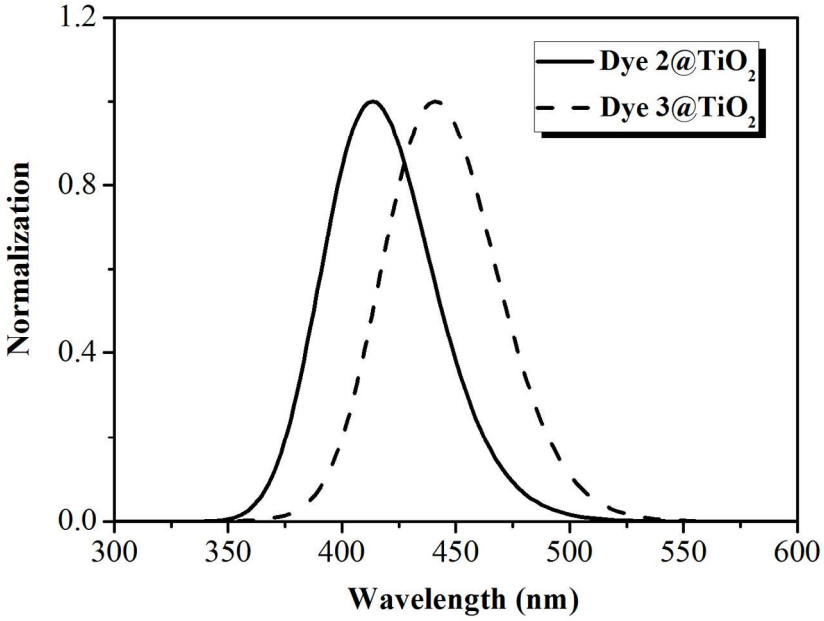

Absorption spectra of Dye 2@TiO2 and Dye 3@TiO2 calculated by TD-CAM-B3LYP/6-31G(d) level in gas phase.
297x208mm (150 x 150 DPI)

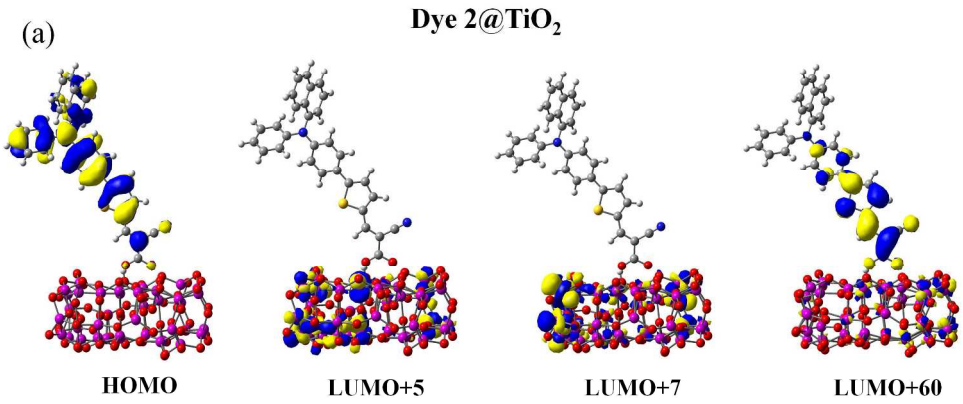

MOs relevant to the transition from S0 to S1 of organic sensitizer adsorbed on the (TiO2)38 in gas phase calculated by TD-CAM-B3LYP/6-31G(d) on DMol3 geometry. (a) Dye 2@TiO2 (b) Dye 3@TiO2.
1249x599mm (62 x 62 DPI)

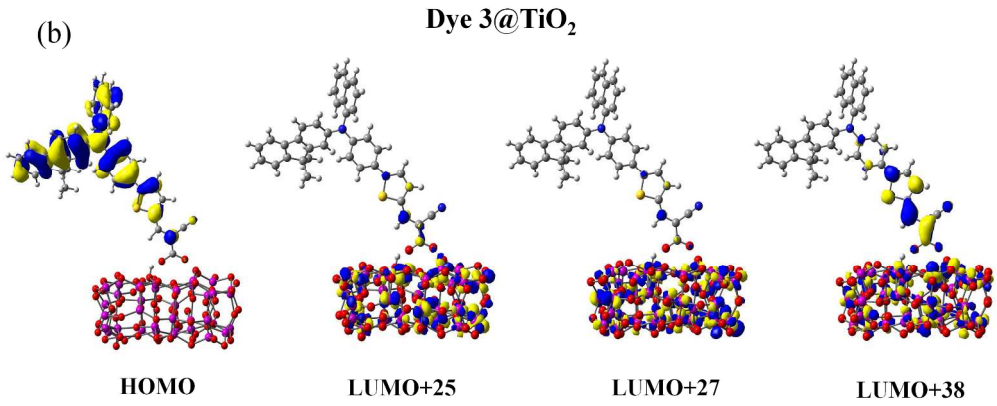

MOs relevant to the transition from S0 to S1 of organic sensitizer adsorbed on the (TiO2)38 in gas phase calculated by TD-CAM-B3LYP/6-31G(d) on DMol3 geometry. (a) Dye 2@TiO2 (b) Dye 3@TiO2.
1249x599mm (62 x 62 DPI)